Eight resonances can be resolved for this interdot tuning with an energy offset ($\Delta\varepsilon$) of about 70 to 120 μeV. Raising the interdot tunneling barrier reduces $\Delta\varepsilon$ (dashed lines), and consequently the number of resonances diminishes to one. As for real dimers, this can be understood by the reduced overlap of the dot wave functions that determines $\Delta\varepsilon$ of corresponding molecular states. The remaining peak is a degenerate multiplet, which unfolds into resonances 2, 3, 4, and 5 as the overlap of two dots' wave functions is increased (indicated by the dashed arrows in Fig. 4B). Furthermore, the energy splitting found is of the same order of magnitude as the one for bonding and antibonding states in coupled dots with one valence electron (*7*). However, here we coherently probe and thus resolve a whole sequence of molecular states.

References and Notes

1. M. Kastner, *Phys. Today* **46** (no. 1), 24 (1993).
2. C. Livermore, C. H. Crouch, R. M. Westervelt, K. L. Campman, A. C. Gossard, *Science* **274**, 1332 (1996).
3. M. Bayer *et al.*, *Science* **291**, 451 (2001).
4. M. N. Leuenberger, D. Loss, *Nature* **410**, 789 (2001).
5. C. J. Myatt *et al.*, *Nature* **403**, 269 (2000).
6. R. H. Blick, D. Pfannkuche, R. J. Haug, K. von Klitzing, K. Eberl, *Phys. Rev. Lett.* **80**, 4032 (1998).
7. A. W. Holleitner, C. R. Decker, H. Qin, K. Eberl, R. H. Blick, *Phys. Rev. Lett.* **87**, e256802 (2001).
8. T. H. Oosterkamp *et al.*, *Nature* **395**, 873 (1998).
9. H. Qin, A. W. Holleitner, K. Eberl, R. H. Blick, *Phys. Rev. B* **64**, R241302 (2001).
10. D. W. Averin, Y. V. Nazarov, in *Single Charge Tunneling*, H. Grabert, M. H. Devoret, Eds., vol. 294 of *NATO ASI Series B* (Plenum, New York, 1992), pp. 217–247.
11. D. Goldhaber-Gordon, H. Shtrikman, D. Mahalu, D. Abusch-Magder, U. Meirav, *Nature* **391**, 156 (1998).
12. S. M. Cronenwett, T. J. Oosterkamp, L. P. Kouwenhoven, *Science* **281**, 540 (1998).
13. F. Simmel, R. H. Blick, J. P. Kotthaus, W. Wegscheider, M. Bichler, *Phys. Rev. Lett.* **83**, 804 (1999).
14. J. Schmid, J. Weis, K. Eberl, K. von Klitzing, *Phys. Rev. Lett.* **84**, 5824 (2000).
15. H. Jeong, A. Chang, M. R. Melloch, *Science* **293**, 2221 (2001).
16. C. A. Büsser, E. V. Anda, A. L. Lima, M. A. Davidovich, G. Chiappe, *Phys. Rev. B* **62**, 9907 (2000).
17. C. W. J. Beenakker, *Phys. Rev. B* **44**, 1646 (1991).
18. F. Hofmann *et al.*, *Phys. Rev. B* **51**, 13872 (1995).
19. Conventional Coulomb blockade oscillations are found to be below the average noise level of $\delta G \leq 0.03$ μS.
20. Fermi's golden rule: The rate of cotunnel events is independent of temperature and only given by $\Gamma = 2\pi/\hbar\Sigma|A|\delta(\varepsilon_1 - \varepsilon_2)$, with $\hbar$, Planck's constant divided by 2π, A as amplitude, and a vanishing energy difference between levels ε_1 and ε_2.
21. T. Fujisawa *et al.*, *Science* **282**, 932 (1998).
22. The filter boxes in the setup are all integrated at room temperature.
23. D. Goldhaber-Gordon *et al.*, *Phys. Rev. Lett.* **81**, 5225 (1998).
24. Underlying conventional Coulomb blockade oscillations start to take over only above $T_{Bath} = 1.2$ K.
25. For energy calibration, from nonlinear transport spectroscopy on each dot individually we find the energy/voltage ratio of each gate and dot to be $\alpha(V_1,\mathrm{dot}_1) = 0.138$ and $\alpha(V_2,\mathrm{dot}_2) = 0.15$.

26. We thank J. v. Delft and F. Wilhelm for stimulating discussions. Supported by the Deutsche Forschungsgemeinschaft, the Bundesministerium für Forschung und Technologie, and the Defense Advanced Research Projects Agency.

25 February 2002; accepted 14 May 2002

Sequence-Specific Molecular Lithography on Single DNA Molecules

Kinneret Keren,[1] Michael Krueger,[1] Rachel Gilad,[1] Gdalyahu Ben-Yoseph,[1,2] Uri Sivan,[1,2] Erez Braun[1,2]*

Recent advances in the realization of individual molecular-scale electronic devices emphasize the need for novel tools and concepts capable of assembling such devices into large-scale functional circuits. We demonstrated sequence-specific molecular lithography on substrate DNA molecules by harnessing homologous recombination by RecA protein. In a sequence-specific manner, we patterned the coating of DNA with metal, localized labeled molecular objects and grew metal islands on specific sites along the DNA substrate, and generated molecularly accurate stable DNA junctions for patterning the DNA substrate connectivity. In our molecular lithography, the information encoded in the DNA molecules replaces the masks used in conventional microelectronics, and the RecA protein serves as the resist. The molecular lithography works with high resolution over a broad range of length scales from nanometers to many micrometers.

Recent advances in the realization of molecular-scale devices (*1*, *2*) highlight their integration into functional circuits as a major challenge. Successful attempts toward this goal include the use of e-beam lithography for wiring carbon nanotubes to form logic circuits (*3*) and the construction of logic gates from nanowire building blocks aligned by flow (*4*).

An alternative route to nanometer-scale electronics relies on molecular recognition and self-assembly. In such a bottom-to-top approach, the information is encoded into the components, which then self-assemble according to that information to form the structure. DNA-programmed assembly is a particularly promising strategy [see, for example, (*5*–*9*)]. We have previously shown that DNA molecules can be uniformly coated with metal to form thin metallic conductive wires that can be attached to macroscopic electrodes by virtue of the DNA molecular recognition properties (*8*, *9*). Molecular electronics, however, requires more elaborate manipulations, including the formation of richer geometries, wire patterning at molecular resolutions, and molecularly accurate device localization. In

[1]Department of Physics, [2]Solid State Institute, Technion-Israel Institute of Technology, Haifa 32000, Israel.

*To whom correspondence should be addressed. E-mail: erez@physics.technion.ac.il

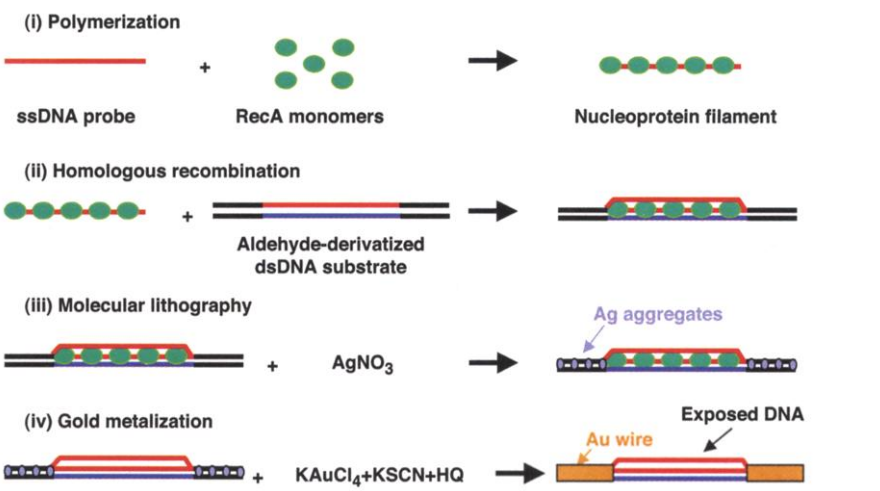

Fig. 1. Schematics of the homologous recombination reaction and molecular lithography. In part (i), RecA monomers polymerize on a ssDNA probe molecule to form a nucleoprotein filament. In part (ii), the nucleoprotein filament binds to an aldehyde-derivatized dsDNA substrate molecule at a homologous sequence. In part (iii), incubation in $AgNO_3$ solution results in the formation of Ag aggregates along the substrate molecule at regions unprotected by RecA. In part (iv), the Ag aggregates serve as catalysts for specific gold deposition, converting the unprotected regions to conductive gold wires. HQ, hydroquinone.

conventional microelectronics, the circuit structure is dictated lithographically. Here, we demonstrate DNA sequence–specific molecular lithography. The molecular lithography uses homologous recombination processes carried out by the RecA protein, operating on double-stranded DNA (dsDNA) substrate molecules (*10*). The information guiding the lithography is encoded in the DNA substrate molecules and in short auxiliary probe DNA molecules. The RecA protein provides the assembling capabilities as well as the resist function. The same process can also be used to create DNA junctions needed for patterning the DNA scaffold connectivity and to localize a molecular-scale object at an arbitrary position along the DNA substrate. That object can later serve as a catalyst for specific growth of a metal island there.

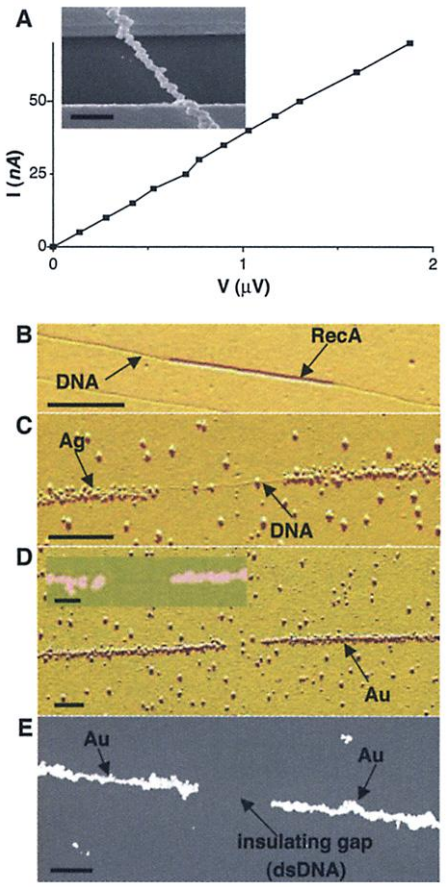

Fig. 2. Sequence-specific molecular lithography on a single DNA molecule. (**A**) Two-terminal current-voltage (*I-V*) curve of a DNA-templated gold wire. The wire's resistivity is 1.5×10^{-7} ohm·m, and that of polycrystalline gold is 2.2×10^{-8} ohm·m. Inset, SEM image of a typical DNA-templated wire stretched between two electrodes deposited by e-beam lithography. Scale bar, 1 μm. (**B**) AFM image of a 2027-base RecA nucleoprotein filament bound to an aldehyde-derivatized λ-DNA substrate molecule. (**C**) AFM image of the sample after Ag deposition. DNA is exposed at the gap between the Ag-loaded sections. (**D**) AFM image of the sample after gold metallization. Inset, close-up image of the gap. The height of the metallized sections is ~50 nm. (**E**) SEM image of the wire after gold metallization. Scale bars in (B) through (E), 0.5 μm; scale bar in inset to (D), 0.25 μm. The distribution in the gap's length is mainly due to variability in DNA stretching on the solid support. The very low background metallization in the SEM images compared with the AFM ones indicates that most of the background is insulating. The DNA molecules were stretched by combing (*22*) on doped silicon wafers passivated by trimethylchlorosilane (Sigma).

Homologous recombination is a protein-mediated reaction by which two DNA molecules, possessing some sequence homology, cross over at equivalent sites. RecA is the major protein responsible for that process in *Escherichia coli* (*10*). In our process, RecA proteins are polymerized on a probe DNA molecule to form a nucleoprotein filament, which is then mixed with the substrate molecules, leading to nucleoprotein-substrate binding at homologous probe-substrate locations, as shown schematically in Fig. 1, parts (i) and (ii). The RecA polymerization on the probe DNA is not sequence specific. The binding specificity of the nucleoprotein filament to the substrate DNA is dictated by the probe's sequence and its homology to the substrate molecule.

Homologous recombination can be harnessed for sequence-specific patterning of DNA metal coating (Fig. 1). An electroless metallization scheme of DNA molecules was developed in which the reducing agent is localized on the DNA substrate. DNA molecules were first aldehyde derivatized by reaction with glutaraldehyde (*11*). This treatment left the DNA intact and biologically active. RecA was then used to localize a 2027-base single-stranded probe molecule on a homologous section in the middle of a 48,502–base pair aldehyde-derivatized λ-DNA substrate

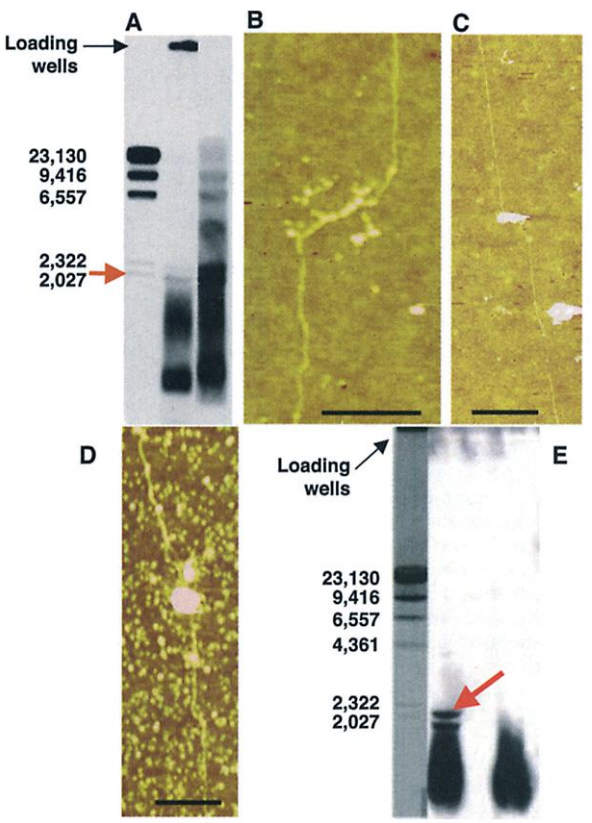

Fig. 3. Sequence-specific localization of labeled nanometer-scale objects on a dsDNA substrate. (**A**) Gel electrophoresis analysis of the recombination reaction [with adenosine 5′-triphosphate (ATP)] between a biotin-labeled 500-base-long ssDNA probe and Hind III–digested λ-DNA. Products were blotted onto a nylon membrane by alkaline capillary transfer and detected with a biotin-chemiluminescent detection kit (KPL, Gaithersburg, MD). Left lane, biotin-labeled Hind III–digested λ-DNA marker; middle lane, recombination reaction; right lane, control reaction without RecA. The fragment homologous to the 500-base ssDNA produces the band marked by a red arrow. The reaction specificity is reflected in the absence of additional bands compared with the control reaction exhibiting extensive spurious binding. The lower bands are 500-base ssDNA strands polymerized with RecA. (**B**) AFM image of a Nanogold-labeled 500-base-long probe bound to a λ-DNA substrate molecule. The height of the central features is 5 nm. Scale bar, 0.2 μm. The recombination reaction was carried out with ATP using a biotin-labeled 500-base-long ssDNA probe and λ-DNA as a substrate. After the recombination reaction, the RecA proteins were decomposed, and the DNA molecules were extracted with phenol-chloroform. The purified reaction products were incubated with streptavidin-conjugated Nanogold for 1 hour at room temperature. (**C**) Sample after electroless gold metallization (*15*) with the Nanogold particles serving as nucleation centers. The metallized object at the center of the DNA molecule is >60 nm high. Scale bar, 1 μm. (**D**) AFM image of a single stretched DNA molecule after ELISA with Nanogold–secondary antibody conjugates (*12*), followed by gold metallization. Scale bar, 0.2 μm. The height of the metallized object at the center is >60 nm, and the background (proteins from the reaction solution that adhere to the surface in the combing process) is <5 nm high. (**E**) Gel electrophoresis of the recombination reaction with Hind III–digested λ-DNA substrate followed by ELISA and chemiluminescent detection. Left lane, Hind III–digested λ-DNA marker; middle lane, recombination reaction; right lane, control reaction with no substrate. There is a specific signal in the reaction lane (marked by a red arrow). The binding of the nucleoprotein filament to the 2027-base fragment leads to a small shift of the band. The additional band below the signal does not correspond to any fragment of the digested λ-DNA, and its origin is unclear.

(*12*). Sequence-specific nucleoprotein binding to the substrate molecule was confirmed by protection against digestion by restriction enzyme (*12*–*14*). The efficiency and specificity of the homologous recombination reaction were not affected by the aldehyde derivatization of the substrate DNA (fig. S2). After the recombination reaction, the molecules were stretched on a passivated silicon wafer. An atomic force microscope (AFM) image (Fig. 2B) shows a RecA nucleoprotein filament bound specifically to the homologous location on the DNA substrate. Next, the sample was incubated in a $AgNO_3$ solution. The reduction of Ag ions by the DNA-bound aldehyde in the unprotected segments of the substrate molecule formed tiny Ag aggregates along the DNA skeleton. The localized RecA proteins, serving as a resist, prevented Ag deposition on the protected aldehyde-derivatized DNA segment and created a gap of exposed sequence between the Ag-loaded segments of the substrate molecule (Fig. 2C). The Ag aggregates served as catalysts for subsequent electroless gold deposition (*15*), which produced two continuous gold wires separated by the predesigned gap (Fig. 2, D and E). Extensive AFM and scanning electron microscopy (SEM) confirm that the metallization gap is located where expected. The position and size of the insulating gap can be tailored by choosing the probe's sequence and length.

The conductivity of the resulting gold wires was characterized by electrode deposition and direct electrical measurements. A SEM image of a DNA-templated wire connecting two electrodes is shown in Fig. 2A (inset). An electrical measurement of that wire, which is a few micrometers in length and 50 to 100 nm wide (Fig. 2A), revealed an ~25-ohm resistance and ohmic characteristics up to currents on the order of 200 nA. The wire conductivity is only one-seventh that of polycrystalline gold, which is four orders of magnitude higher than our previous DNA-templated Ag wires (*8*, *9*). The localization of the reducing agent (aldehyde) on the DNA scaffold results in very low background metallization (this is evident in the SEM images in Fig. 2, A and E, which, unlike the AFM images, distinguish between metallic and nonmetallic background). This metallization process is thus superior to other reduction schemes in the literature (*16*).

In our molecular lithography concept, exposed sequences of dsDNA serve as addresses for localizing molecular objects. A RecA-driven recombination reaction was used to localize arbitrary labeled molecular objects at specific locations along the dsDNA substrate. The specificity (*17*) in localizing a biotin-labeled, 500-base single-stranded DNA (ssDNA) probe on a fragmented λ-DNA substrate is shown in Fig. 3A. The probe is homologous to one of the restriction fragments (marked by a red arrow). The probe binds specifically to that fragment, and negligible amounts of nonspecific binding are seen elsewhere. In contrast, the control reaction without RecA (Fig. 3A, right lane) exhibited extensive nonspecific binding. The labeled probe remained bound to the substrate after deproteinization and can thus be used for localizing objects. The products of the same reaction were used with intact λ-DNA substrate. The deproteinized reaction products were incubated with streptavidin-conjugated 1.4-nm gold particles (Nanogold, Nanoprobes, Yaphank, New York). The streptavidin-conjugated Nanogold binds specifically to the biotinylated probe. An AFM image (Fig. 3B) shows the Nanogold-bound ssDNA probe localized on the substrate dsDNA, and Fig. 3C shows that electroless gold deposition (*15*) results in gold growth around the catalyzing Nanogold particles. As demonstrated by Sato *et al.* (*18*), gold clusters can be used as single electron transistors.

The RecA proteins bound to the DNA substrate can also be used for localizing molecular objects and selective growth of a metallic island, using antibodies in a process analogous to standard enzyme-linked immunosorbent assay (ELISA). First, primary antibodies to RecA were reacted with the sample (*12*). Next, gold particles conjugated to secondary antibodies with high affinity to the primary antibodies were localized on them. Gold metallization resulted in a metallic cluster localized on the DNA substrate (Fig. 3D). The specificity of the reaction was confirmed with a fragmented λ-DNA substrate (as in Fig. 3A). The reaction products were separated by gel electrophoresis, transferred to a membrane, and detected by chemiluminescence (using horseradish peroxidase–conjugated secondary antibodies), as shown in Fig. 3E (*12*). A clear signal appeared only at the band corresponding to the DNA fragment homologous to the probe (marked by a red arrow in Fig. 3E). Detection with Nanogold–secondary antibody conjugates and successive gold metallization led to similar results.

Finally, we show how the same mechanism can be harnessed to generate the molecularly accurate DNA junctions required for the creation of an elaborate DNA scaffold. Artificial DNA junctions have been demonstrated with hybridization, but they require precise design and ssDNA (oligonucleotide) synthesis (*19*). RecA generates junctions between any two dsDNA molecules having homologous regions (*20*). Junction formation is depicted schematically in Fig. 4B. Two types of DNA molecules, 15 and 4.3 kilobase pairs (kbp) long, were prepared (*12*). The short molecule is homologous to a 4.3-kbp segment at one end of the long molecule. RecA was first polymerized on the short molecule and then reacted with the long molecule. The recombination reaction led to the formation of a stable three-armed junction with two 4.3-kbp-long arms and an 11-kbp-long third arm. Junction formation was confirmed by

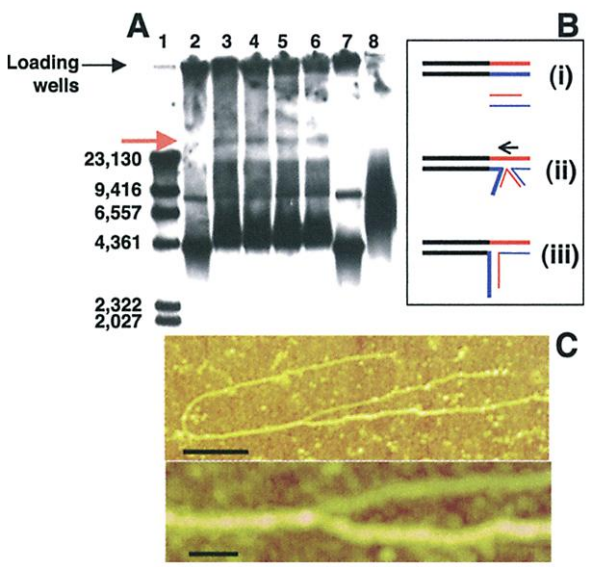

Fig. 4. Stable three-armed junction. (**A**) RecA-promoted homologous junction formation (*12*) between biotin-labeled 4.3-kbp-long and unlabeled 15-kbp-long dsDNA molecules. The reaction products for different reaction times (lane 3, 30 min; lane 4, 60 min; lane 5, 120 min; lane 6, 210 min) were electrophoresed, blotted onto a nylon membrane, and detected with a chemiluminescent-biotin detection kit. Lane 1, biotin-labeled Hind III–digested λ-DNA marker. Lanes 2 and 7 are control reactions without RecA (lane 2, 5 min; lane 7, 210 min). Lane 8 is a control reaction without ATP (210 min). The band marked by a red arrow contains stable three-armed junctions. Additional bands correspond to labeled 4.3-kbp molecules and their 8.6-kbp spontaneously formed dimers. At long reaction times (lanes 5 and 6), the junction band intensity decreases because of junction-junction interaction leading to the formation of more complex structures that remain in the loading wells. (**B**) Different steps in junction formation. Step (i) shows building blocks (15-and 4.3-kbp dsDNA). The latter molecule is completely homologous to one end of the former molecule and has a 50-base-long sticky end (*12*). Step (ii) shows pairing at homologous sequences and branch migration. Step (iii) shows the final product, a stable three-armed junction. (**C**) AFM images of a three-armed junction, which can serve as a scaffold for a three-terminal device. Scale bars, 0.25 μm (top) and 50 nm (bottom). The lengths of the arms are as expected, considering the variations due to interaction with the surface in the combing process.

biotin labeling of the 4.3-kbp molecules and gel electrophoresis. An additional specific band (marked by a red arrow) that was absent in the control reactions is shown in Fig. 4A. By excising the additional band from the gel, extracting the DNA, and spreading it on a solid support, we verified that the specific band comprises DNA junctions. AFM images of such a junction are shown in Fig. 4C. These junctions can serve as a template for a three-terminal device.

The realization of sequence-specific molecular lithography constitutes an important step toward integrated DNA-templated electronics. Homologous recombination by RecA operates on scales varying between a few bases (nanometers) to thousands of bases (micrometers) with essentially single-base accuracy (~0.3 nm). Thus, our molecular lithography can operate on a broad range of length scales with essentially nanometer resolution. The various molecular lithography processes demonstrated above can be carried out sequentially; for example, junction definition followed by specific metallization of the unprotected junction's arms and colloid localization at the junction represent three levels of lithography. Molecular lithography can be applied to other DNA-programmed constructs (e.g., for mechanical applications). The resist function provided by the RecA protein can most likely be extended to operations other than metallization, because the protein apparently blocks the access of even small molecules (Ag ions in the present case) to the DNA substrate.

References and Notes

1. C. M. Lieber, *Sci. Am.* **285**, 58 (September 2001).
2. C. Joachim, J. K. Gimzewski, A. Aviram, *Nature* **408**, 541 (2000).
3. A. Bachtold, P. Hadley, T. Nakanishi, C. Dekker, *Science* **294**, 1317 (2001).
4. Y. Huang *et al.*, *Science* **294**, 1313 (2001).
5. C. M. Niemeyer, *Curr. Opin. Chem. Biol.* **4**, 609 (2000).
6. J. J. Storhoff, C. A. Mirkin, *Chem. Rev.* **99**, 1849 (1999).
7. E. Winfree, F. Liu, L. A. Wenzler, N. C. Seeman, *Nature* **394**, 539 (1998).
8. E. Braun, Y. Eichen, U. Sivan, G. Ben-Yoseph, *Nature* **391**, 775 (1998).
9. Y. Eichen, E. Braun, U. Sivan, G. Ben-Yoseph, *Acta Polym.* **49**, 663 (1998).
10. M. M. Cox, *Prog. Nucleic Acid Res. Mol. Biol.* **63**, 311 (2000).
11. λ-DNA (Promega, Madison, WI) was precipitated with ethanol to remove tris traces and dissolved in 25 mM Hepes buffer (pH 7.5) with 4 mM MgAc (final DNA concentration of 0.1 μg/μl). The DNA was incubated with 0.2% glutaraldehyde for 20 min at room temperature and then for 20 min on ice. Excess glutaraldehyde was filtered out by overnight dialysis. Aldehyde-derivatized DNA molecules were stretched on doped passivated silicon and then incubated in the dark with a 0.1 M solution of $AgNO_3$ (purity 99.9%, Carlo Erba Reagents, Milan, Italy) in 25% ammonia buffer (pH 10.5) (titrated with 70% HNO_3) at room temperature for a few hours. Gold metallization (*15*) was performed after gently washing off excess Ag with water.
12. Materials and methods are available as supporting online material on *Science* Online.
13. L. J. Ferrin, R. D. Camerini-Otero, *Science* **254**, 1494 (1991).
14. W. Szybalski, *Curr. Opin. Biotechnol.* **8**, 75 (1997).
15. A unit volume of KSCN (60 mg/ml) was mixed with a unit volume of $KAuCl_4$ (23 mg/ml) and centrifuged for 1 min at 4000*g*. The supernatant was removed, and the precipitate was mixed with 8 unit volumes of 1 M phosphate buffer (pH 5.5). Finally, a unit volume of hydroquinone (5.5 mg/ml) was added. The sample was instantly immersed in this solution and left to incubate for 0.5 to 3 min (*21*).
16. J. Richter *et al.*, *Adv. Mater.* **12**, 507 (2000).
17. S. M. Honigberg, R. B Jagadeeshwar, C. M. Radding, *Proc. Natl. Acad. Sci. U.S.A.* **83**, 9586 (1986).
18. T. Sato, H. Ahmed, D. Brown, B. F. G. Johnson, *J. Appl. Phys.* **82**, 696 (1997).
19. C. Mao, S. Weiqiong, N. C. Seeman, *J. Am. Chem. Soc.* **121**, 5437 (1999).
20. B. Muller, I. Burdett, S. C. West, *EMBO J.* **11**, 2685 (1992).
21. Y. Eichen, U. Sivan, E. Braun, PCT WO0025136 (international patent application) (1999) (http://ep.espacenet.com).
22. D. Bensimon, A. J. Simon, V. Croquette, A. Bensimon, *Phys. Rev. Lett.* **74**, 4754 (1995).

23. We acknowledge financial support by the European Commission 5th Framework Program project number IST-1999-1309S, the Israel Science Foundation, and the Rosenbloom Foundation. K.K. acknowledges support by the Clore Foundation.

Supporting Online Material

www.sciencemag.org/cgi/content/full/297/5578/72/DC1
Materials and Methods
Figs. S1 and S2

25 February 2002; accepted 13 May 2002

Global Distribution of Neutrons from Mars: Results from Mars Odyssey

W. C. Feldman,[1]* W. V. Boynton,[2] R. L. Tokar,[1] T. H. Prettyman,[1] O. Gasnault,[1] S. W. Squyres,[3] R. C. Elphic,[1] D. J. Lawrence,[1] S. L. Lawson,[1] S. Maurice,[4] G. W. McKinney,[1] K. R. Moore,[1] R. C. Reedy[1]

Global distributions of thermal, epithermal, and fast neutron fluxes have been mapped during late southern summer/northern winter using the Mars Odyssey Neutron Spectrometer. These fluxes are selectively sensitive to the vertical and lateral spatial distributions of H and CO_2 in the uppermost meter of the martian surface. Poleward of ±60° latitude is terrain rich in hydrogen, probably H_2O ice buried beneath tens of centimeter-thick hydrogen-poor soil. The central portion of the north polar cap is covered by a thick CO_2 layer, as is the residual south polar cap. Portions of the low to middle latitudes indicate subsurface deposits of chemically and/or physically bound H_2O and/or OH.

Neutron spectroscopy can be used to survey planetary bodies for hydrogen (*1*). The epithermal neutron energy range (0.4 to about 500 keV) is most sensitive for this purpose. Measurements of thermal (<0.4 eV) and epithermal neutron fluxes also provide unique information about the existence and thickness of deposits of CO_2 (*2*). Such deposits are expected to cover both martian polar caps during their respective winter months (*3–5*), and CO_2 is also thought to blanket the residual south polar cap of Mars (*5–7*).

A component of the Gamma-Ray Spectrometer (GRS) aboard Mars Odyssey is the Neutron Spectrometer (NS) (*8*, *9*). For the purposes of our initial global survey of neutrons produced by Galactic cosmic rays that leak away from Mars, we used data collected between 20 March and 18 April 2002, covering areocentric Sun longitudes between about 345° and 360° (late in southern summer/northern winter). An estimation of the abundance and stratigraphy of hydrogen near the south martian pole using gamma-ray and neutron data is presented separately (*10*).

The NS consists of a cubical block of boron-loaded plastic scintillator that is segmented into four individual prism-shaped sensors (*9*). During mapping, the four sensors are oriented with one facing down toward Mars, one facing in the forward direction nearly along the spacecraft's velocity vector (V_{sc}), one facing backward, nearly antiparallel to V_{sc}, and one facing upward (*11*). The difference in counting rates between the forward- and backward-facing sensors is a reliable estimate of the counting rate across the thermal energy band because the backward sensor measures the epithermal and spacecraft components. The downward-facing sen-

[1]Los Alamos National Laboratory, Los Alamos, NM 87545, USA. [2]University of Arizona, Lunar Planetary Laboratory, Tucson, AZ 85721, USA. [3]Cornell University, Center for Radiophysics and Space Research, Ithaca, NY 14853, USA. [4]Observatoire Midi-Pyrénées, 31400 Toulouse, France.

*To whom correspondence should be addressed. E-mail: wfeldman@lanl.gov